

# Effect of Multiaxiality on the Stress Rupture Properties of P92 Steel

Lakshmiprasad Maddi<sup>1,\*</sup>, Srinivas R Gavinola<sup>2</sup>, Atul Ballal<sup>3</sup>

\* lakshmiprasad.m@gmrit.edu.in

<sup>1</sup> Department of Basic Sciences and Humanities, GMRT, Rajam, Andhra Pradesh, INDIA, 532127

<sup>2</sup> Department of Physics, Presidency University, Yelahanka, Bengaluru, Karnataka, INDIA, 560064

<sup>3</sup> Department of Metallurgical and Materials Engineering, Visvesvaraya National Institute of Technology, Nagpur, Maharashtra, INDIA, 440010

Received: November 2023

Revised: April 2024

Accepted: May 2024

DOI: 10.22068/ijmse.3442

**Abstract:** High thermal conductivity and low coefficient of thermal expansion make P92 a candidate material for Ultra Super Critical (USC) power plant piping. Microstructural features viz., high dislocation density, lath martensitic microstructure, and fine precipitates of  $M_{23}C_6$  and  $MX$  ( $X = C, N$ ) contribute towards the high rupture strength. However, most components are typically subjected to multiaxial stress conditions; either metallurgical (weldments) or mechanical (change in the dimension). The present work involves stress rupture testing of circumferential 60° V-notch specimens in the 300 – 375 MPa range at 650°C. A notch strengthening effect was observed; with rupture times ranging from 200 – 1300 h. Scanning electron microscopy (SEM) fractography revealed a mixed mode of fracture with brittle fracture observed at the notch root, while ductile fracture was seen at the centre of the specimen.

**Keywords:** Multiaxiality, Notched specimen, Stress rupture, Transient creep.

## 1. INTRODUCTION

Per capita power consumption is one of the important factors to measure the growth of a country/economy. Thermal power plants are the major contributors to the ever-increasing demands of energy by humankind. However, due to the combustion of fossil fuels, greenhouse gases viz.,  $CO_2$  are emitted that are harmful to the earth's climate. An increase in the efficiency of thermal power plants is the need of the hour. Therefore, the development of appropriate materials towards creep strength has always been an evolving area that has demanded continuous efforts from the scientific community.

P92 steels (9Cr– 0.5 Mo– 1.8 W) exhibit the microstructure of tempered martensite. Characteristic features such as high dislocation density, and fine lath width contribute towards dislocation strengthening together with fine precipitates (precipitate hardening) making the material suitable for piping applications in Ultra Super Critical (USC) power plants [1–5]. However, tempered martensite microstructure evolves with time via decreased dislocation density and increased lath width and precipitate size. In practice, most parts involve either a change in cross-sectional area or a weld. The former acts as a mechanical stress concentration

site [6–9], while the latter acts as a metallurgical stress concentration site, inducing a degree of multiaxiality.

Ragab *et al.* [10] attempted to model the creep crack growth of a Grade 91 weldment using the continuum damage mechanics model. Goyal *et al.* [11] studied the effects of multiaxial stress on the rupture life of 9Cr– 1Mo steels by machining U-notch of varying notch root radii. Reduction in Von–Mises stress was found to enhance rupture life [12]. Han *et al.* [13] also studied creep cavitation in P91 material under the presence of multiaxial stresses (U-notch specimens). Creep fracture was explained in the context of size, and frequency of cavities. The combined action of equivalent stress and triaxiality resulted in the formation of creep cavities, with a higher number of cavities present away from the notch root. Though the effect of notches is widely studied in fatigue testing, very few studies are available on multiaxial creep testing of P92 steel [14], which necessitates more extensive investigations. The present study is one such attempt wherein the stress rupture response of the material is studied under multiaxial loading conditions by machining a circumferential V-notch.

## 2. EXPERIMENTAL PROCEDURES

P92 material is procured in the form of plates

from Mishra Dhatu Nigam (MIDHANI) Hyderabad, India. The composition of the test material is shown in Table 1. P92 bars were then cut using EZEECUT wire EDM into bars, which were subsequently heat-treated and machined into test samples. Figure 1 represents the various steps involved in sample preparation. Table 2 represents the geometry of the circumferential 60° V-notched specimen. Stress rupture tests were performed as per ASTM standard E252 at 650°C in the stress range of 300–375 MPa using STAR creep testing systems, in Mumbai, India. JEOL 6380 A SEM was used for metallographic and fractographic studies. Villela's reagent (1 g picric acid + 5 ml HCl + 100 ml ethanol) was used as an etchant.

### 3. RESULTS AND DISCUSSION

#### 3.1. Creep Behavior

Figure 2 shows the creep curves of the samples tested in the range of 300 – 375 MPa. Notch strengthening behavior was observed when compared to the plain specimen (Appendix A1). An increase in stress level leads to a reduction in the rupture time. The strain rate varied by one

order for the sample tested at 375 MPa ( $\times 10^{-5}$ ) when compared to the remaining samples ( $\times 10^{-6}$ ). According to Han et al. [13], the coarsening of precipitates and reduction in the dislocation density was attributed as the possible reasons for the high creep rate noted at high stress and high temperature. All the samples exhibited predominant primary stage creep followed by tertiary creep (Table 3). The secondary creep region (steady state creep) was negligible. Higher rupture strain was noted at a higher stress level (375 MPa), while lower rupture strain was noted for the lower stress level (300 MPa). Also, an increase in rupture strain rate by an order of magnitude was observed at 375 MPa.

#### 3.2. Microstructural Studies

Figure 3 shows the initial microstructure of the sample exhibiting lath martensitic structure with  $M_{23}C_6$  carbides decorating the grain/packet/lath boundaries. No Laves phase formation was observed as evident from lack of contrast in back-scattered electron imaging. Due to the small size of MX carbonitrides they were not sufficiently resolved in SEM.

**Table 1.** Chemical composition of P92 steel

| Element | C    | Si    | Mn    | P     | S     | Cr   | Ni    | Mo    | Al    | Cu    | V     | Nb    | W    |
|---------|------|-------|-------|-------|-------|------|-------|-------|-------|-------|-------|-------|------|
| Wt. %   | 0.11 | 0.308 | 0.417 | 0.017 | 0.003 | 9.38 | 0.086 | 0.529 | 0.013 | 0.017 | 0.175 | 0.067 | 1.97 |



**Fig. 1.** Sample preparation

**Table 2.** Geometry of the test sample

| Gauge length              | Gross diameter | Notch depth (d) | Notch root radius (r) | Notch acuity ratio (d/r) | Stress concentration factor ( $k_t$ ) |
|---------------------------|----------------|-----------------|-----------------------|--------------------------|---------------------------------------|
| 50                        | 5              | 0.86            | 0.20                  | 4.3                      | 3.2                                   |
| *All dimensions are in mm |                |                 |                       |                          |                                       |

**Table 3.** Comparison of stress rupture parameters

| Sample          | Fraction of time spent |                   | Rupture Strain | Rupture Strain Rate ( $h^{-1}$ ) |
|-----------------|------------------------|-------------------|----------------|----------------------------------|
|                 | In Primary stage       | In tertiary stage |                |                                  |
| 300 MPa/ 1242 h | 84                     | 15                | 0.005          | $4.025 \times 10^{-6}$           |
| 325 MPa/ 895 h  | 83                     | 16                | 0.007          | $7.93 \times 10^{-6}$            |
| 375 MPa/ 269 h  | 88                     | 11                | 0.0077         | $2.9 \times 10^{-5}$             |

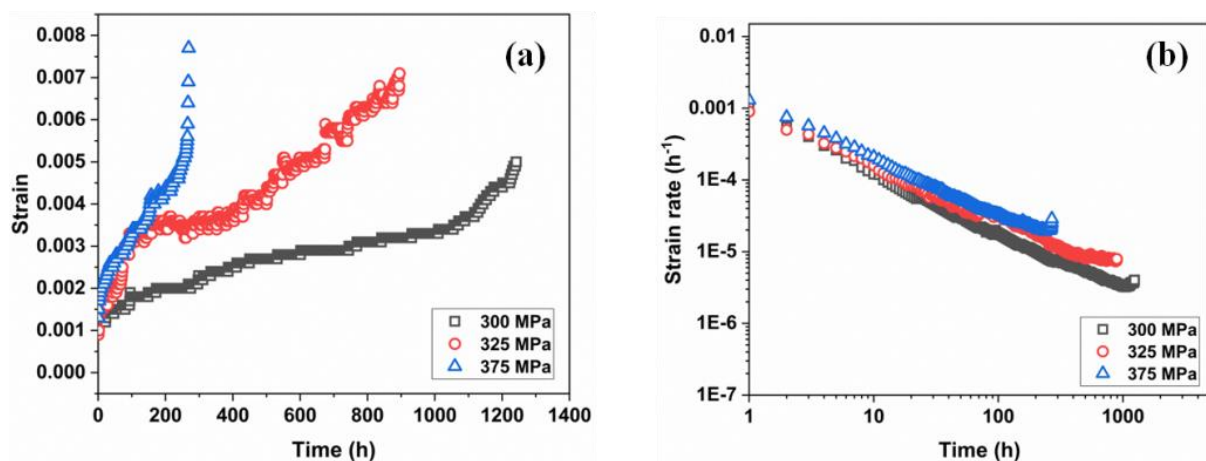


Fig. 2. (a) Creep curves (b) Variation in minimum creep rate with time

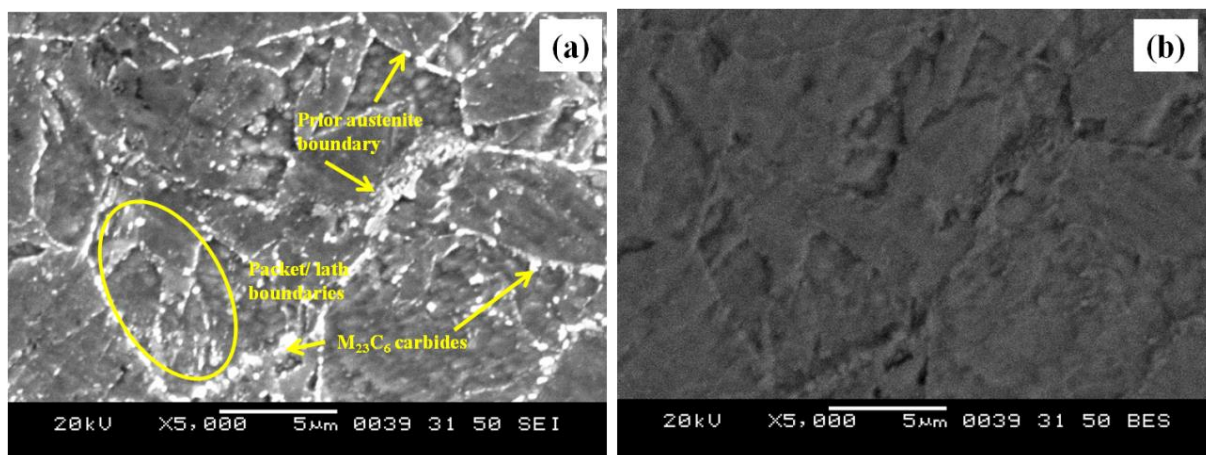


Fig. 3. Initial microstructure of the sample (a) Secondary electron (b) Back Scattered electron imaging

Figure 4 shows the micrographs of ruptured samples, wherein M<sub>23</sub>C<sub>6</sub> carbides (bright spots) occupy the grain/packet/lath boundaries. Backscattered electron (BSE) imaging revealed the presence of Laves phases (Fe<sub>2</sub>Mo/Fe<sub>2</sub>W) that become visible due to their large atomic number. Precipitation of Laves phases occurs through two mechanisms (a) Nucleation at a coherent interface followed by growth along an incoherent interface (b) Nucleation adjacent to M<sub>23</sub>C<sub>6</sub> carbides and growth along an incoherent interface [15–17]. Earlier work of the authors also [18–19] proved the second mechanism to be dominant in P92 steels. J Cui et al. [20] studied the effect of creep stress on Laves phases. Under creep stress, mobile dislocations move from the lath boundary interior to the boundary regions. During the process, they also drag W/Mo atoms along with them to the precipitates at the boundary, thereby resulting in precipitate coarsening. Figure 4 indicates the increased coarsening of Laves

phases with exposure time. Previous studies of the authors [18] under uniaxial creep stress also indicated the accelerated evolution of the microstructure, wherein Laves phases precipitated after 1000 h of creep exposure. However, in the current study involving multiaxial stresses, Laves phases precipitated at a much earlier time of 269 h. Similar observations related to the accelerated growth of the precipitates under multiaxial stresses were also reported in the literature [21–22].

### 3.3. Fractography

Under multiaxial loading, rupture life was found to vary with applied stress [11] as,

$$t = M \sigma_{\text{rep}}^{-m}$$

where  $M$  and  $m$  are the damage parameters.  $\sigma_{\text{rep}}$  denotes the representative stress, defined as the same level of stress applied for a plain specimen that results in the same rupture time.



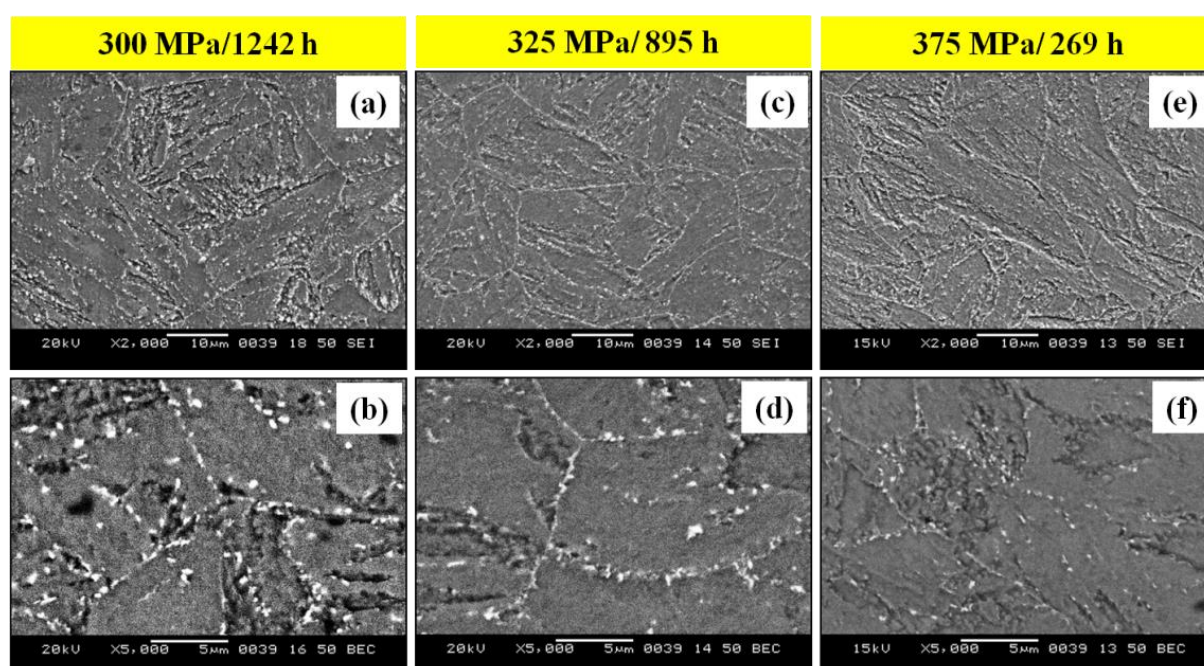


**Fig. 4.** SEM images of (a) 300 MPa/1242 h (c) 325 MPa/895 h (e) 375 MPa/269 h. (b, d, f) represent the corresponding Back Scattered Electrons (BSE) images of (a, c, e)

Typically,  $\sigma_{rep}$  is a combination of maximum principal stress and von-mises stress, the latter being dominant in deciding the fracture behavior. Maximum creep damage will be observed at the notch root and center of a notched specimen with the notch root acting as initiation site. Hence, fractographic studies were performed at two different sites of the ruptured specimens, (1) at the notch root and (2) at the center, to study the effect of multiaxial stress (Figure 5).

The brittle fracture was observed at the notch root which was characterized by distinct facets (a', b', c'). Dimple morphology seen in a'', b'', c'' establish a ductile mode of fracture at the center of the specimen. Figure 5 (a'', b'' and c'') also confirms the presence of large-sized cavities/voids at lower stress (300 MPa), while the fracture was largely fibrous (small voids) at a higher stress level of 375 MPa.

Goyal et al. [12] also modelled variations in maximum principal stress with distance from the notch root for 2.25Cr-1Mo steels. It was established that cavity nucleation and growth were a direct reflection of the variations in maximum principal stress. It is noteworthy at this juncture, that, cavity nucleation and growth were seen as the prime contributors for creep damage at lower stresses [13], while

creep cracks were attributed to be the reason for creep damage at high stresses. Figure 4 also supports the above observation, wherein, coarsened Laves phases eventually lead to large size cavities, that initiate and promote rupture. On the other hand, rupture at high stresses might be due to tear ridges resulting in crack initiation and growth. A large crack observed in Figure 5 (c) validates the above proposed assumption.

#### 4. CONCLUSIONS

The rupture behavior of P92 steel was studied under multiaxial stresses. The notch strengthening effect was observed which may be attributed to stress redistribution at the notch root. Precipitation of Laves phases was observed adjacent to  $M_{23}C_6$  carbides on the lath boundaries. A mixed mode of fracture was seen in all three samples due to multiaxial stress distribution.

#### ACKNOWLEDGEMENT

The authors are thankful to Dr MD Mathew and Dr K Laha of the Indira Gandhi Center for Atomic Research (IGCAR), Kalpakkam, Tamilnadu, India for their guidance and valuable discussions.

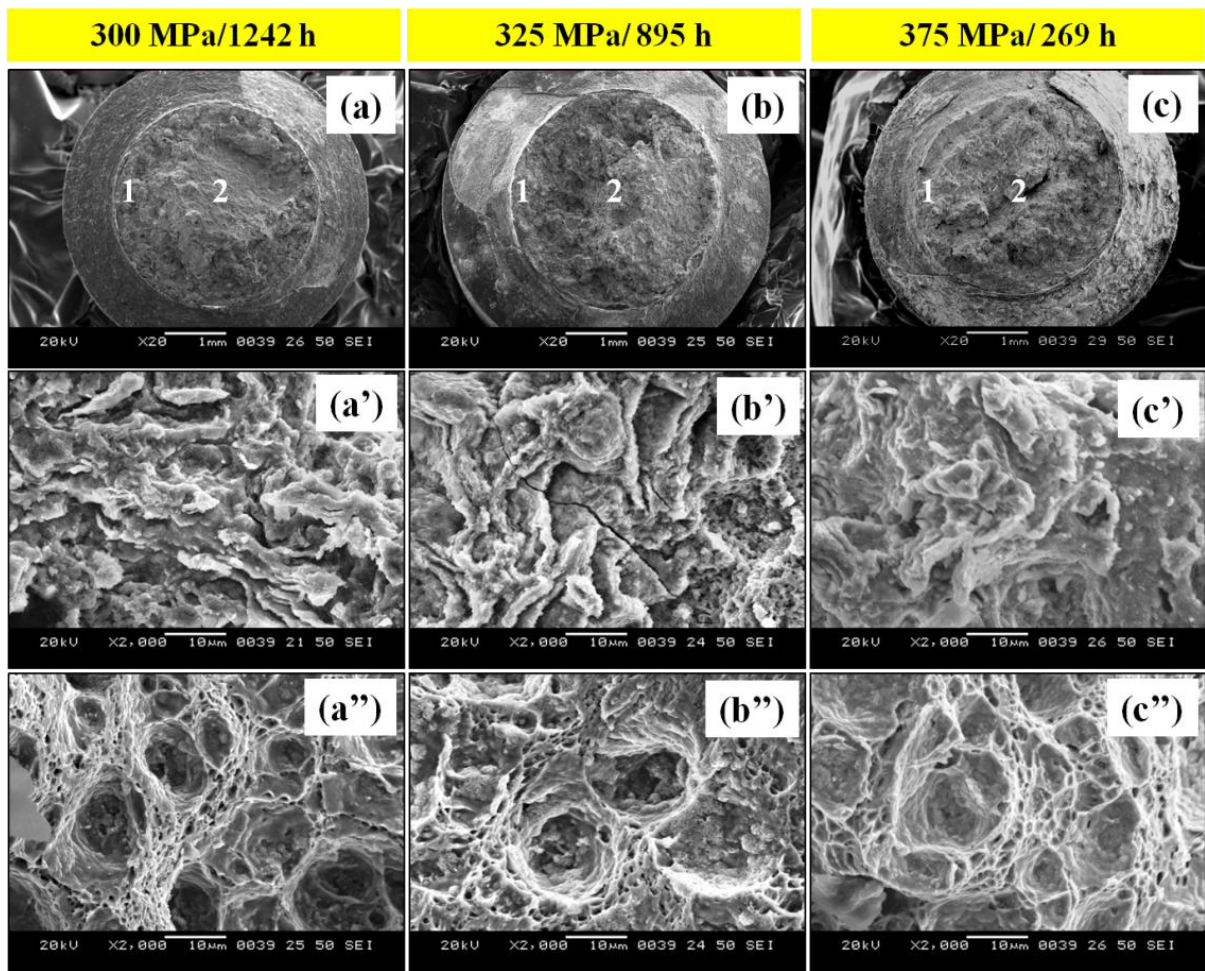
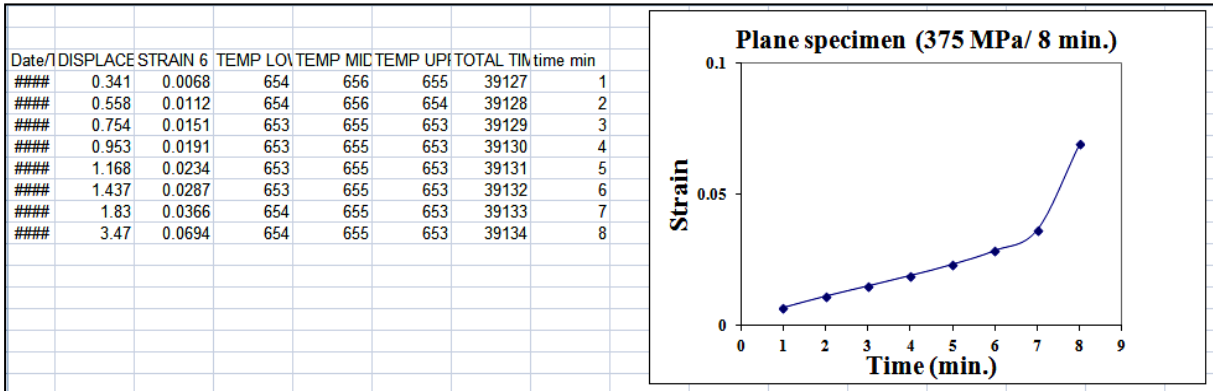


**Fig. 5.** Fractographs of samples (a) 300 MPa/1242 h (c) 325 MPa/895 h (e) 375 MPa/269 h. a', b, c' represents fractographs at the notch root (position 1) and a'', b'', c'' show fractographs at the specimen centre (position 2)

APPENDIX

A1. Rupture data for Plane specimen tested at 375 MPa/ 650°C.



REFERENCES

[1]. Alang N.A., Nikbin K., “An analytical and numerical approach to multiscale ductility

constraint-based model to predict uniaxial/multiaxial creep rupture and cracking rates.” Int. J. Mech. Sci., 2018, 135, 342-352.



- [2]. Zhao L., Jing H., Xu L., Han Y., Xiu J., "Analysis of creep crack growth behavior of P92 steel welded joint by experiment and numerical simulation." *Mater. Sci. Eng. A.*, 2012, 558, 119-128.
- [3]. Alang N.A., Nikbin K., "A new approach to predict creep rupture of Grade 92 steel under multiaxial stress states." *Int. J. Mech. Sci.*, 2019, 163, 105096.
- [4]. Chang Y., Xu H., Ni Y., Lan X., Li H., "Research on representative stress and fracture ductility of P92 steel under multiaxial creep." *Eng. Fail. Anal.*, 2016, 59, 140-150.
- [5]. Chang Y., Xu H., Ni Y., Lan X., Li H., "The effect of multiaxial stress state on creep behavior and fracture mechanism of P92 steel." *Mater. Sci. Eng. A.*, 2015, 636, 70-76.
- [6]. Goyal S., Laha K., Das C.R., Panneerselvi S., Mathew M.D., "Effect of constraint on creep behavior of 9Cr-1Mo steel." *Metall. Mater. Trans. A.*, 2014, 45A, 619-632.
- [7]. Pandey C., Mahapatra M.M., Kumar P., Saini N., "Effect stress state and notch geometry on tensile properties and fracture mechanism of creep strength enhanced ferritic P91 steel." *J. Nucl. Mater.*, 2018, 498, 176-186.
- [8]. Sahoo K.C., Goyal S., Paul V.T., Laha K., "Effect of notch depth on creep rupture behaviour of 304HCu austenitic stainless steel." *Mater. High Temp.*, 2020, 37(5), 295-304.
- [9]. Mao J., Li X., Bao S., Ge R., Yan L., "The experimental and numerical studies on multiaxial creep behavior of Inconel 783 at 700°C." *Int. J. Pres. Ves. Pip.*, 2019, 173, 133-146.
- [10]. Ragab R., Parker J., Li M., Liu T., Sun W., "Creep crack growth modelling of Grade 91 vessel weldments using a modified ductility based damage model." *Eur. J. Mech. A-Solid.*, 2022, 91, 104424.
- [11]. Goyal S., Laha K., "Creep life prediction of 9Cr-1Mo steel under multiaxial state of stress." *Mater. Sci. Eng. A.*, 2014, 615, 348-360.
- [12]. Goyal S., Laha K., Das C.R., Selvi S.P., Mathew M.D., "Finite element analysis of uniaxial and multiaxial state of stress on creep rupture behaviour of 2.25Cr-1Mo steel." *Mater. Sci. Eng. A.*, 2013, 563, 68-77.
- [13]. Han K., Ding H., Fan X., Li W., Lv Y., Feng Y., "Study of the creep cavitation behaviour of P91 steel under different stress states and its effect on high-temperature creep properties." *J. Mater. Res. Technol.*, 2022, 20, 47-59.
- [14]. Vaidya A., Ballal A., Yadav H.K., Peshwe D., "Stress rupture studies of V – notched grade 92 steel for high temperature applications." *Proceed. Struct. Integr.*, 2019, 14, 410-415.
- [15]. Prat O., Garcia J., Rojas D., Sauthoff G., Inden G., "The role of Laves phase on microstructure evolution and creep strength of novel 9% Cr heat resistant steels." *Intermetallics.*, 2013, 32, 362-372.
- [16]. Fedoseeva A., Nikitin I., Tkachev E., Mishnev R., Dudova N., Kaibyshev R., "Effect of Alloying on the Nucleation and Growth of Laves Phase in the 9-10% Cr-3% Co Martensitic Steels during Creep." *Metals.*, 2020, 11(1), 60.
- [17]. Dudova N., Mishnev R., Kaibyshev R., "Creep behavior of a 10% Cr heat-resistant martensitic steel with low nitrogen and high boron contents at 650°C." *Mater. Sci. Eng. A.*, 2019, 766, 138353.
- [18]. Maddi L., Deshmukh G.S., Ballal A.R., Peshwe D.R., Paretkar R.K., Laha K., Mathew M.D., "Effect of Laves phase on the creep rupture properties of P92 steel." *Mater. Sci. Eng. A.*, 2016, 668, 215-223.
- [19]. Cui H., Sun F., Chen K., Zhang L., Wan R., Shan A., Wu J., "Precipitation behavior of Laves phase in 10% Cr steel X12CrMoWVNbN10-1-1 during short-term creep exposure." *Mater. Sci. Eng. A.*, 2010, 527 29-30, 7505-7509.
- [20]. Cui J., Kim I.S., Kang C.Y., Miyahara K., "Creep stress effect on the precipitation behavior of Laves phase in Fe– 10% Cr–6% W alloys." *ISIJ Int.* 2001, 41(4), 368-371.
- [21]. Niu, T.Y., Zhao P., Zhu G., Gong J.G., Xuan F.Z., "Stress state dependent creep damage behavior of 9-12% Cr steel notched components." *Mater. Sci. Eng. A.*, 2021, 804, 140762.
- [22]. Ni, Y., Xu H., Chang Y., Mao X., "Research on elastic-plastic creep damage

of notched P92 steel specimens.” *Mater. High. Temp.*, 2018, 35(4), 335-342.